Progress In Electromagnetics Research M, Vol. 47, 1–12, 2016

Visualization of Eddy Current Distributions for Arbitrarily Shaped Coils Parallel to a Moving Conductor Slab

Toshiya Itaya[1, *], Koichi Ishida[2], Yasuo Kubota[3], Akio Tanaka[4], and Nobuo Takehira[2]

Abstract—To visualize eddy current distribution (ECD) of an arbitrarily shaped coil arranged parallel to a moving conductor slab, an exact theoretical solution is derived using an analytical method based on the double Fourier transform method. The arbitrarily shaped coil is regarded as a plane coil of a single turn, and both DC and AC excitation currents can be applied. Furthermore, ECD charts are obtained when the conductor slab is moving. We calculate some examples with respect to a circular coil, rectangular coil, and triangular coil and show the effect of coil excitation frequency and speed of the conductor on ECDs. Results show that the eddy current generated in the moving conductor slab is composed of current induced by the excitation frequency and conductor speed.

1. INTRODUCTION

Eddy current applications have produced various industry technologies, e.g., eddy current testing, induction heating and eddy current sensors. Eddy current testing is used to detect defects in structural materials such as steel, aluminum, titanium and carbon-fiber-reinforced plastic [1]. Induction heating is used in commercial cooking and heat treatment. Eddy current sensors are widely used for displacement [2], conductivity [3] and thickness measurements [4]. These measurements use the change in eddy currents magnitude to measure the physical quantity of interest. However, because the eddy current cannot be measured directly, it is difficult to determine the eddy current distribution (ECD). Furthermore, when a conductor is moved, the behavior of the eddy current becomes complicated. Therefore, theoretical analysis to clarify the ECD is strongly desired. The behavior of an eddy current strongly depends on factors such as coil shape, excitation frequency, conductor speed and conductor properties [5]. These complex dependencies have thus far prevented the development of a precise theoretical analysis of ECD.

Dodd and Deeds presented an analytical solution for the eddy current density induced by the circular coil arranged parallel to a conductor slab using the integral of the Bessel function [6]. Thus, the basic phenomenon of the relationship between eddy current density and skin depth has been described. Panas and Papayiannakis represented the magnetic vector potential by a filamentous elliptical coil in a Cartesian coordinate system; the solution of partial differential equations is obtained in the form of a 2D Fourier transform, which then allows the inverse Fourier transform of the magnetic flux density and eddy current density to be calculated [7]. Analytical expressions are also given for the ECD of a circular coil arranged perpendicular [8] or tilted [9] to the conductor slab. Theodoulidis and Kriezis obtained an analytical solution for ECD of a rectangular coil by introducing a concept called secondary vector potential [10]. When ECD is considered for conductors in motion, the skin effect due to velocity

Received 12 January 2016, Accepted 24 February 2016, Scheduled 15 March 2016

* Corresponding author: Toshiya Itaya (itaya@info.suzuka-ct.ac.jp).

[1] Department of Electronic and Information Engineering, National Institute of Technology, Suzuka College, Suzuka 510-0294, Japan. [2] Department of Mechanical and Electrical Engineering, National Institute of Technology, Tokuyama College, Shunan 745-8585, Japan. [3] Kohan Kogyo Co., Ltd., Kudamatu 744-0011, Japan. [4] Department of Electrical Engineering, National Institute of Technology, Ube College, Ube 755-8585, Japan.

is affected is known. When a DC excitation coil is moved, using the second vector potential in place of the magnetic vector potential, the analytical solution can be shown in Fourier space by a 2D Fourier transform [11]. Panas and Kriezis represented an analytical solution for the case when the DC excitation filamentary rectangular coil is moved by a 3D Fourier transform with respect to time and space; these results are numerically computed by a fast Fourier algorithm from the inverse Fourier transform [12]. When both the AC excitation coil and conductor slab are moved, the eddy current generated by them should be considered. An analytical method have been already proposed based on the double Fourier transform method that considers the case of the conductor slab moving in relation to the rectangular coil [13].

In the present study, a new technique to visualize the ECD in a conductor slab due to an arbitrarily shaped coil is proposed. The arbitrarily shaped coil is regarded as a plane coil of a single turn, and both DC and AC excitation current can be applied. Furthermore, ECD charts were visualized when the conductor slab is moving. Some examples with respect to a circular coil, rectangular coil and triangular coil were calculated and the effect of coil excitation frequency and the speed of the conductor on visualized ECDs were shown.

2. THEORETICAL ANALYSIS

Figure 1 shows the geometry of the analytical model. The surface of the conductor is matched to the $z = 0$ plane. The distance between the coil and slab is z_0. To facilitate magnetic field analysis, the following assumptions are made. The moving conductor is isotropic and infinitely wide. The coil is a one-turn coil and carries current I with a known effective rms value and angular frequency ω. The coil wire is assumed to be infinitely thin. The conductivity σ, permeability μ and conductor speed $\bar{v} = (v_x, v_y, 0)$ are constant. In the quasi-steady state, the displacement current is negligible and the following equations are obtained:

$$\nabla \times \bar{H} = \bar{J} \tag{1}$$

$$\nabla \times \bar{E} = -\frac{\partial \bar{B}}{\partial t} \tag{2}$$

$$\nabla \cdot \bar{B} = 0 \tag{3}$$

where

$$\nabla \cdot \bar{J} = 0 \tag{4}$$

Since conductor speed $\bar{v} = (v_x, v_y, 0)$ is very small in comparison with light velocity, the next

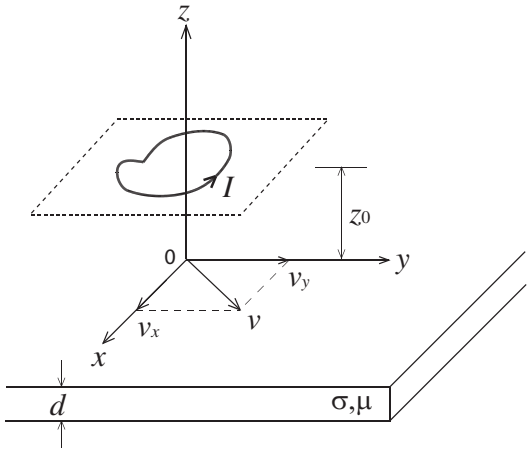

Figure 1. Geometry of analytical model which comprises arbitrarily shaped coil and moving conductor slab.

equations are obtained:

$$\bar{J} = \sigma(\bar{E} + \bar{v} \times \bar{B}) \tag{5}$$

$$\bar{B} = \mu \bar{H} \tag{6}$$

To solve Maxwell's equation, a double Fourier transform and its inverse are introduced as follows

$$b(\xi, \eta, z) = \int_{-\infty}^{\infty} \int_{-\infty}^{\infty} B(x, y, z) e^{j(x\xi + y\eta)} dx dy \tag{7}$$

$$B(x, y, z) = \frac{1}{4\pi^2} \int_{-\infty}^{\infty} \int_{-\infty}^{\infty} b(\xi, \eta, z) e^{-j(x\xi + y\eta)} d\xi d\eta \tag{8}$$

2.1. Magnetic Flux Densities Produced by an Arbitrarily Shaped Planar Coil

According to Appendix A, the x-, y- and z-components of the magnetic flux density $\bar{B}$ in the conductor slab are given by

$$\begin{aligned} B_x = {} & \frac{\mu_0 \mu_r I}{8\pi^2} \int_{-\infty}^{\infty} \int_{-\infty}^{\infty} \frac{\xi}{\eta\left(1 - e^{2\gamma d}\right)} \left[\left\{ -\left(1 + \lambda_0\right) e^{2\gamma d} + \nu_0 \right. \right. \\ & \left. \left. \times e^{\left(\gamma - \sqrt{\xi^2 + \eta^2}\right) d} \right\} e^{\gamma z} + \left\{ 1 + \lambda_0 - \nu_0 e^{\left(\gamma - \sqrt{\xi^2 + \eta^2}\right) d} \right\} e^{-\gamma z} \right] \\ & \times e^{-z_0 \sqrt{\xi^2 + \eta^2}} S\left(\xi, \eta\right) e^{-j(x\xi + y\eta)} d\xi d\eta \end{aligned} \tag{9}$$

$$\begin{aligned} B_y = {} & \frac{\mu_0 \mu_r I}{8\pi^2} \int_{-\infty}^{\infty} \int_{-\infty}^{\infty} \frac{1}{1 - e^{2\gamma d}} \left[\left\{ -\left(1 + \lambda_0\right) e^{2\gamma d} + \nu_0 \right. \right. \\ & \left. \left. \times e^{\left(\gamma - \sqrt{\xi^2 + \eta^2}\right) d} \right\} e^{\gamma z} + \left\{ 1 + \lambda_0 - \nu_0 e^{\left(\gamma - \sqrt{\xi^2 + \eta^2}\right) d} \right\} e^{-\gamma z} \right] \\ & \times e^{-z_0 \sqrt{\xi^2 + \eta^2}} S\left(\xi, \eta\right) e^{-j(x\xi + y\eta)} d\xi d\eta \end{aligned} \tag{10}$$

$$\begin{aligned} B_z = {} & j \frac{\mu_0 \mu_r I}{8\pi^2} \int_{-\infty}^{\infty} \int_{-\infty}^{\infty} \frac{\xi^2 + \eta^2}{\eta\gamma\left(1 - e^{2\gamma d}\right)} \left[\left\{ -\left(1 + \lambda_0\right) e^{2\gamma d} + \nu_0 \right. \right. \\ & \left. \left. \times e^{\left(\gamma - \sqrt{\xi^2 + \eta^2}\right) d} \right\} e^{\gamma z} - \left\{ 1 + \lambda_0 - \nu_0 e^{\left(\gamma - \sqrt{\xi^2 + \eta^2}\right) d} \right\} e^{-\gamma z} \right] \\ & \times e^{-z_0 \sqrt{\xi^2 + \eta^2}} S\left(\xi, \eta\right) e^{-j(x\xi + y\eta)} d\xi d\eta \end{aligned} \tag{11}$$

Here, $S(\xi, \eta)$ is called the shape function [14] and defined as

$$S\left(\xi, \eta\right) = \sum_{i=1}^{n} \int_{x'_{i-1}}^{x'_i} e^{j\{x'\xi + f_i(x')\eta\}} dx' \tag{12}$$

where $\mu_r = \mu / \mu_0$ and

$$\gamma = \sqrt{\xi^2 + \eta^2 - j\sigma\mu_0\mu_r \left(v_x \xi + v_y \eta\right) + j\omega\sigma\mu_0\mu_r} \tag{13}$$

$$\lambda_0 = \frac{\left\{\gamma^2 - {\mu_r}^2 \left(\xi^2 + \eta^2\right)\right\} \left(1 - e^{-2\gamma d}\right)}{\left(\gamma + \mu_r \sqrt{\xi^2 + \eta^2}\right)^2 - \left(\gamma - \mu_r \sqrt{\xi^2 + \eta^2}\right)^2 e^{-2\gamma d}} \tag{14}$$

$$\nu_0 = \frac{4\mu_r \gamma \sqrt{\xi^2 + \eta^2} e^{(\sqrt{\xi^2 + \eta^2} - \gamma) d}}{\left(\gamma + \mu_r \sqrt{\xi^2 + \eta^2}\right)^2 - \left(\gamma - \mu_r \sqrt{\xi^2 + \eta^2}\right)^2 e^{-2\gamma d}} \tag{15}$$

Quantities ξ and η are integration variables of the Fourier transform; furthermore, λ_0 and ν_0 depend on the angular frequency of the excitation current, the conductor thickness, materials and speed.

2.2. Eddy Current Densities Produced by an Arbitrarily Shaped Planar Coil

The x- and y-components of eddy current density $\bar{J}$ produced in the conductor slab by the arbitrarily shaped planar coil can be described as

$$J_x = \frac{1}{\mu_0\mu_r}\left(\frac{\partial B_z}{\partial y} - \frac{\partial B_y}{\partial z}\right) \tag{16}$$

$$J_y = \frac{1}{\mu_0\mu_r}\left(\frac{\partial B_x}{\partial z} - \frac{\partial B_z}{\partial x}\right) \tag{17}$$

which can be solved as follows

$$\begin{aligned} J_x = & -\frac{I}{8\pi^2}\int_{-\infty}^{\infty}\int_{-\infty}^{\infty}\frac{\gamma^2-\xi^2-\eta^2}{\gamma\left(1-e^{2\gamma d}\right)}\left[\left\{-\left(1+\lambda_0\right)e^{2\gamma d}+\nu_0\right.\right. \\ & \left.\left.\times\, e^{\left(\gamma-\sqrt{\xi^2+\eta^2}\right)d}\right\}e^{\gamma z}-\left\{1+\lambda_0-\nu_0 e^{\left(\gamma-\sqrt{\xi^2+\eta^2}\right)d}\right\}e^{-\gamma z}\right] \\ & \times\, e^{-z_0\sqrt{\xi^2+\eta^2}}S\left(\xi,\,\eta\right)e^{-j(x\xi+y\eta)}d\xi d\eta \end{aligned} \tag{18}$$

$$\begin{aligned} J_y = & \frac{I}{8\pi^2}\int_{-\infty}^{\infty}\int_{-\infty}^{\infty}\frac{\xi\left(\gamma^2-\xi^2-\eta^2\right)}{\eta\gamma\left(1-e^{2\gamma d}\right)}\left[\left\{-\left(1+\lambda_0\right)e^{2\gamma d}+\nu_0\right.\right. \\ & \left.\left.\times\, e^{\left(\gamma-\sqrt{\xi^2+\eta^2}\right)d}\right\}e^{\gamma z}-\left\{1+\lambda_0-\nu_0 e^{\left(\gamma-\sqrt{\xi^2+\eta^2}\right)d}\right\}e^{-\gamma z}\right] \\ & \times\, e^{-z_0\sqrt{\xi^2+\eta^2}}S\left(\xi,\,\eta\right)e^{-j(x\xi+y\eta)}d\xi d\eta \end{aligned} \tag{19}$$

2.3. Stream Function

The eddy current density obtained above in conjunction with the stream function is used to visualize ECD. The eddy current streamline in the xy plane is described by

$$\frac{dy}{dx} = \frac{\mathrm{Re}\left(J_y\right)}{\mathrm{Re}\left(J_x\right)} \tag{20}$$

Therefore, we have

$$\mathrm{Re}\left(J_y\right)dx - \mathrm{Re}\left(J_x\right)dy = 0 \tag{21}$$

where operator Re( ) returns the real part of the arguments and provides the instantaneous value of eddy current density. Stream function $U(x, y)$ in the xy plane is given by

$$U\left(x,\,y,\,z\right) = \mathrm{Re}\left(\int J_y dx\right) = k \;= \text{constant} \tag{22}$$

or

$$U\left(x,\,y,\,z\right) = \mathrm{Re}\left(\int -J_x dy\right) = k \;= \text{constant} \tag{23}$$

Equation (21) may be used in either Equation (22) or (23). This paper uses Equation (22) in Equation (21). Since the eddy current in a conductor slab changes over time, it is a function of time t. Therefore, stream function $U(x, y, z, t)$ is given by

$$U\left(x,\,y,\,z,\,t\right) = \mathrm{Re}\left(\int J_y dx\sqrt{2}e^{j\omega t}\right) = \sqrt{2}\left\{\mathrm{Re}\left(\int J_y dx\right)\cos\omega t - \mathrm{Im}\left(\int J_y dx\right)\sin\omega t\right\} = k \tag{24}$$

where operator Im( ) returns the imaginary part of the arguments and provides the instantaneous value of eddy current density. In the above equations, constant k is obtained by substituting point (x, y) with the curve connecting point (x, y) having the equivalent value k. Thus, the distribution diagram of the

eddy current at time t on z plane is obtained. In addition, the integral in Equation (24) may be written as

$$\int J_y dx = j\frac{I}{8\pi^2}\int_{-\infty}^{\infty}\int_{-\infty}^{\infty}\frac{-j\sigma\mu_0\mu_r\left(v_x\xi+v_y\eta\right)+j\omega\sigma\mu_0\mu_r}{\eta} \times Te^{-z_0\sqrt{\xi^2+\eta^2}}S\left(\xi,\,\eta\right)e^{-j(x\xi+y\eta)}d\xi d\eta \tag{25}$$

$$T = \frac{1}{\gamma\left(1-e^{2\gamma d}\right)}\left[\left\{-\left(1+\lambda_0\right)e^{2\gamma d}+\nu_0 e^{\left(\gamma-\sqrt{\xi^2+\eta^2}\right)d}\right\}e^{\gamma z} - \left\{1+\lambda_0-\nu_0 e^{\left(\gamma-\sqrt{\xi^2+\eta^2}\right)d}\right\}e^{-\gamma z}\right] \tag{26}$$

2.4. Shape Function

The shape function depends on the coil shape. When the coil is divided into three pieces of closed curve, each closed curve carries the same current, as shown in Figure 2. If they are described as $y' = f_1(x')$, $f_2(x')$ and $f_3(x')$, the shape function is obtained as follows by integrating counter clockwise

$$S\left(\xi,\,\eta\right) = \int_{x'_0}^{x'_1} e^{j\{x'\xi+f_1(x')\eta\}}dx' + \int_{x'_1}^{x'_2} e^{j\{x'\xi+f_2(x')\eta\}}dx' + \int_{x'_2}^{x'_3} e^{j\{x'\xi+f_3(x')\eta\}}dx' \tag{27}$$

Next, the shape functions for a circular coil, rectangular coil and triangular coil using Equation (27) are derived. The center of the coils is the centroid of the shape.

2.4.1. Circular coil (Figure 3)

The functions for regions 1 and 2 are expressed as

$$\begin{cases} y' = f_1\left(x'\right) = -\sqrt{a^2-\left(x'\right)^2} \\ y' = f_2\left(x'\right) = \sqrt{a^2-\left(x'\right)^2} \end{cases} \tag{28}$$

Therefore, from Equation (27), shape function $S(\xi,\eta)$ is given as

$$S\left(\xi,\,\eta\right) = \int_{-a}^{a} e^{j\{x'\xi+f_1(x')\eta\}}dx' + \int_{a}^{-a} e^{j\{x'\xi+f_2(x')\eta\}}dx' = -j\frac{2\pi a\eta}{\sqrt{\xi^2+\eta^2}}J_1\left(a\sqrt{\xi^2+\eta^2}\right) \tag{29}$$

where $J_1(\ )$ is a Bessel function.

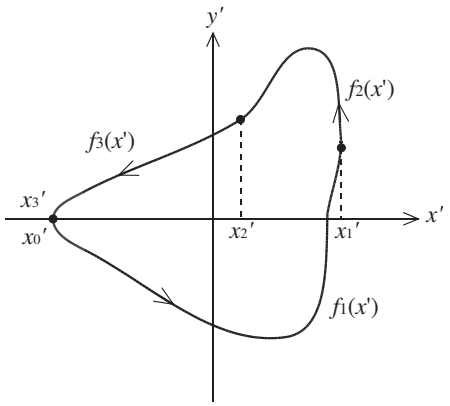

Figure 2. Arbitrarily shaped planar coil which is divided into three pieces of closed curve.

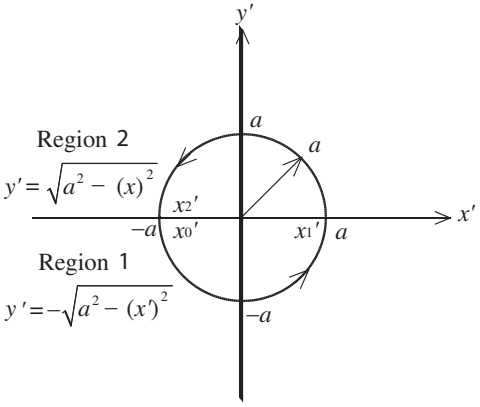

Figure 3. Circular coil with radius a.

2.4.2. Rectangular coil (Figure 4)

The functions for regions 1 and 2 are expressed as

$$\begin{cases} y' = f_1(x') = -b \\ y' = f_2(x') = b \end{cases} \tag{30}$$

Therefore, from Equation (27), shape function $S(\xi, \eta)$ is given as

$$S(\xi,\, \eta) = \int_{-a}^{a} e^{j\{x'\xi + f_1(x')\eta\}} dx' + \int_{a}^{-a} e^{j\{x'\xi + f_2(x')\eta\}} dx' = -j\frac{4}{\xi}\sin(a\xi)\sin(b\eta) \tag{31}$$

2.4.3. Triangular coil (Figure 5)

The functions for lines 1, 2 and 3 are expressed as follows:

$$\begin{cases} y' = f_1(x') = -\dfrac{b}{3} \\ y' = f_2(x') = -\dfrac{b}{a}x' + \dfrac{2}{3}b \\ y' = f_3(x') = \dfrac{b}{a}x' + \dfrac{2}{3}b \end{cases} \tag{32}$$

Therefore, from Equation (27), shape function $S(\xi, \eta)$ is given as

$$\begin{aligned} S(\xi,\, \eta) \;=\; & \int_{-a}^{a} e^{j\{x'\xi + f_1(x')\eta\}} dx' + \int_{a}^{0} e^{j\{x'\xi + f_2(x')\eta\}} dx' + \int_{0}^{-a} e^{j\{x'\xi + f_3(x')\eta\}} dx' \\ =\; & e^{-j\frac{b}{3}\eta}\left[\frac{2}{\xi}\sin(a\xi) + \frac{2a}{a^2\xi^2 - b^2\eta^2}\left\{b\eta\sin(b\eta) - a\xi\sin(a\xi)\right\}\right. \\ & \left. + j\frac{2ab\eta}{a^2\xi^2 - b^2\eta^2}\left\{\cos(a\xi) - \cos(b\eta)\right\}\right] \end{aligned} \tag{33}$$

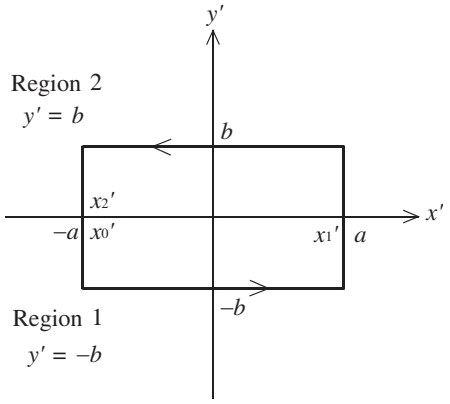

Figure 4. Rectangular coil with length $2a$ and width $2b$.

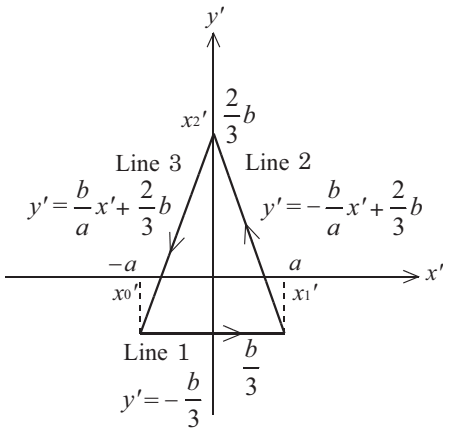

Figure 5. Triangular coil with base length $2a$ and height b.

3. RESULTS AND DISCUSSION

From Equation (24), the visualized ECD as a function of excitation frequency and conductor speed are obtained. The y (x)-direction corresponds to the horizontal (vertical) axis. ECD is given for $z = 0$ and $t = 0$. In the expression for ECD, k is a relative value related to the density and size of the eddy

Table 1. Specifications of coils.

Circular coil	Rectangular coil	Triangular coil
$a = 25\,\text{mm}$	$a = 50\,\text{mm}$	$a = 25\,\text{mm}$
	$b = 25\,\text{mm}$	$b = 75\,\text{mm}$

Table 2. Specifications of conducting slab.

Aluminum
$\sigma = 3 \times 10^7\,\text{S/m}$
$d = 10\,\text{mm}$
$\mu_r = 1$

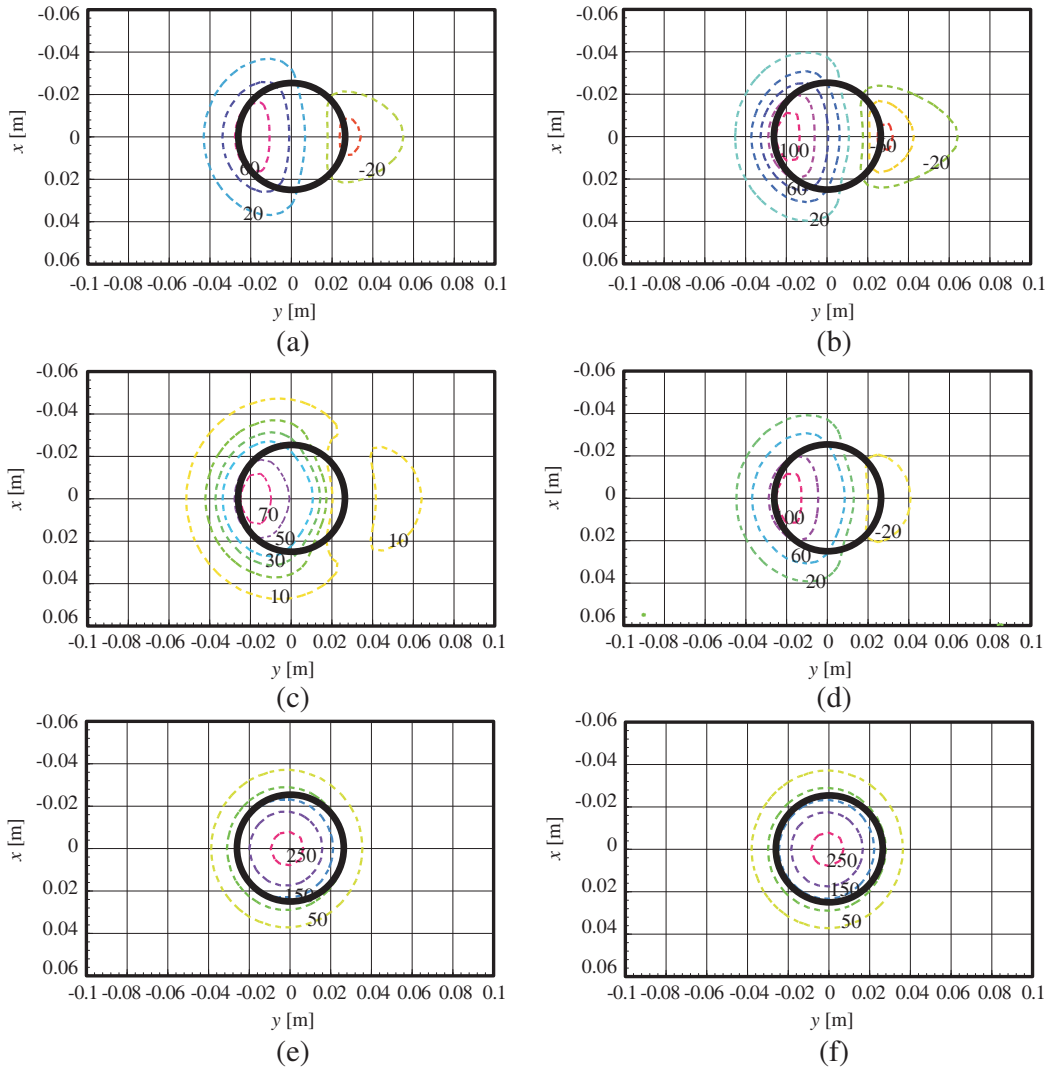

Figure 6. ECDs for a circular coil when excitation frequency and conductor speed change. (a) DC, $v = 10\,\text{m/s}$, (b) DC, $v = 20\,\text{m/s}$, (c) $f = 100\,\text{Hz}$, $v = 10\,\text{m/s}$, (d) $f = 100\,\text{Hz}$, $v = 20\,\text{m/s}$, (e) $f = 1000\,\text{Hz}$, $v = 10\,\text{m/s}$ and (f) $f = 1000\,\text{Hz}$, $v = 20\,\text{m/s}$.

current. The thick line represents the coil line (i.e., Figures 6–8). The distance between the coil and the conducting slab is $z_0 = 10\,\text{mm}$. The coil was excited by a 1 A current. The excitation frequency was set to 0 (DC), 100 and 1000 Hz. Table 1 shows the specifications of the coils and Table 2 shows the specifications of the conducting slab. The conductor speed was set to $v_y = v = 10$ and $20\,\text{m/s}$. The conductor slab was allowed to move only in the y-direction ($v_x = 0$). A positive value represents the magnitude of the eddy current in the opposite direction to the direction of the coil current, whereas

a negative value represents the magnitude of the eddy currents in the same direction relative to the direction of the coil current.

Figure 6 shows ECD for a circular coil. At DC and $v = 10\,\mathrm{m/s}$ or $20\,\mathrm{m/s}$, two current vortexes with different polarities were generated in the y-direction. At $f = 100\,\mathrm{Hz}$ and $v = 10\,\mathrm{m/s}$, two current vortexes with similar polarities were generated in the y-direction. At $v = 20\,\mathrm{m/s}$, their polarities became opposite. At $v = 20\,\mathrm{m/s}$, their polarities became opposite. At $f = 1000\,\mathrm{Hz}$, only a single vortex was generated. At this frequency, the size of the eddy current increased, but the speed did not affect the ECD.

Figure 7 shows ECD for a rectangular coil. At DC and $v = 10\,\mathrm{m/s}$ or $20\,\mathrm{m/s}$, two current vortexes with different polarities were generated in the y-direction. At $f = 100\,\mathrm{Hz}$ and $v = 10\,\mathrm{m/s}$, two current vortexes with similar polarities were generated in the y-direction. At $v = 20\,\mathrm{m/s}$, their polarities became opposite. At $f = 1000\,\mathrm{Hz}$, only a single vortex was generated. At this frequency, the size of the eddy current increased, but the speed did not affect the ECD. The single vortex had a smooth shape with rounded corners of the coil.

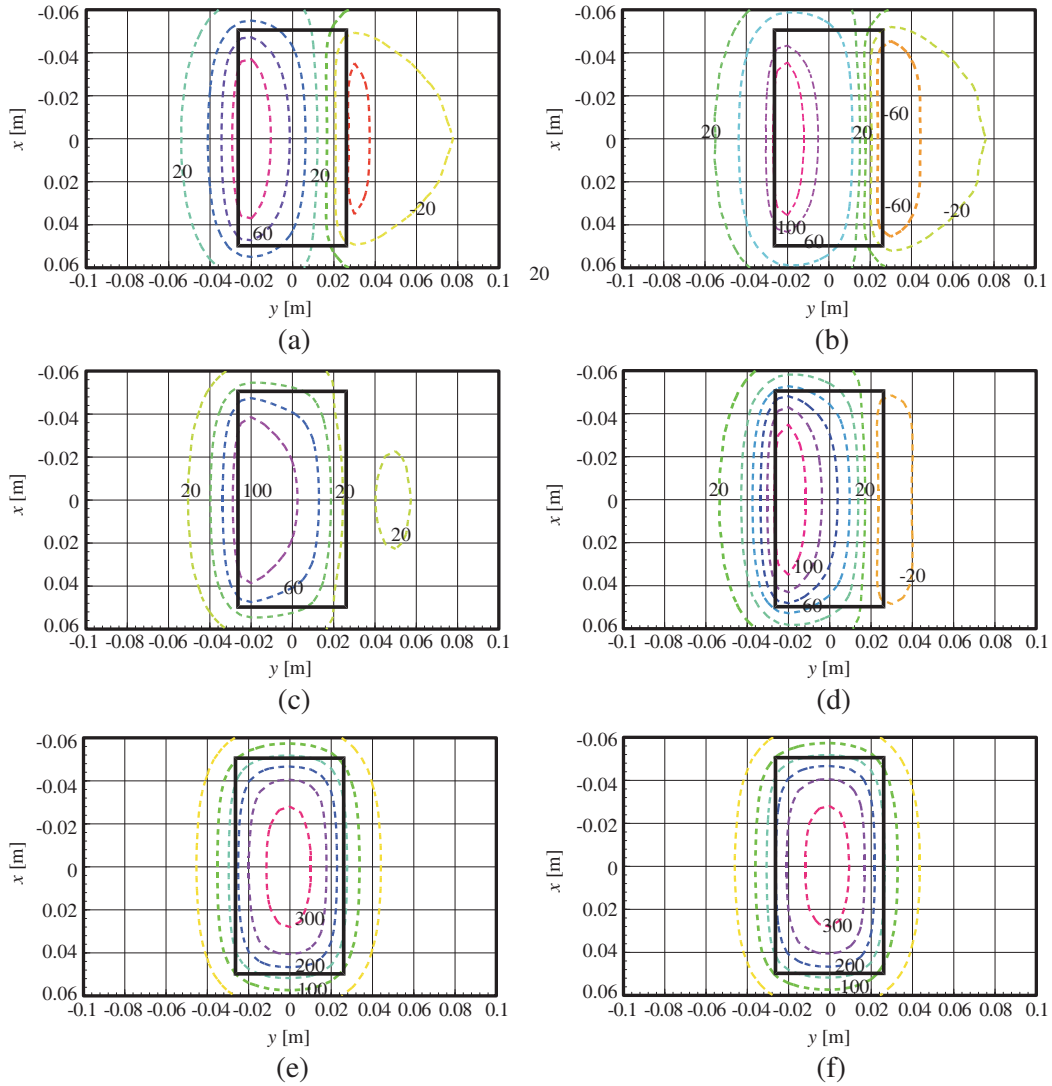

Figure 7. ECDs for a rectangular coil when excitation frequency and conductor speed change. (a) DC, $v = 10\,\mathrm{m/s}$, (b) DC, $v = 20\,\mathrm{m/s}$, (c) $f = 100\,\mathrm{Hz}$, $v = 10\,\mathrm{m/s}$, (d) $f = 100\,\mathrm{Hz}$, $v = 20\,\mathrm{m/s}$, (e) $f = 1000\,\mathrm{Hz}$, $v = 10\,\mathrm{m/s}$ and (f) $f = 1000\,\mathrm{Hz}$, $v = 20\,\mathrm{m/s}$.

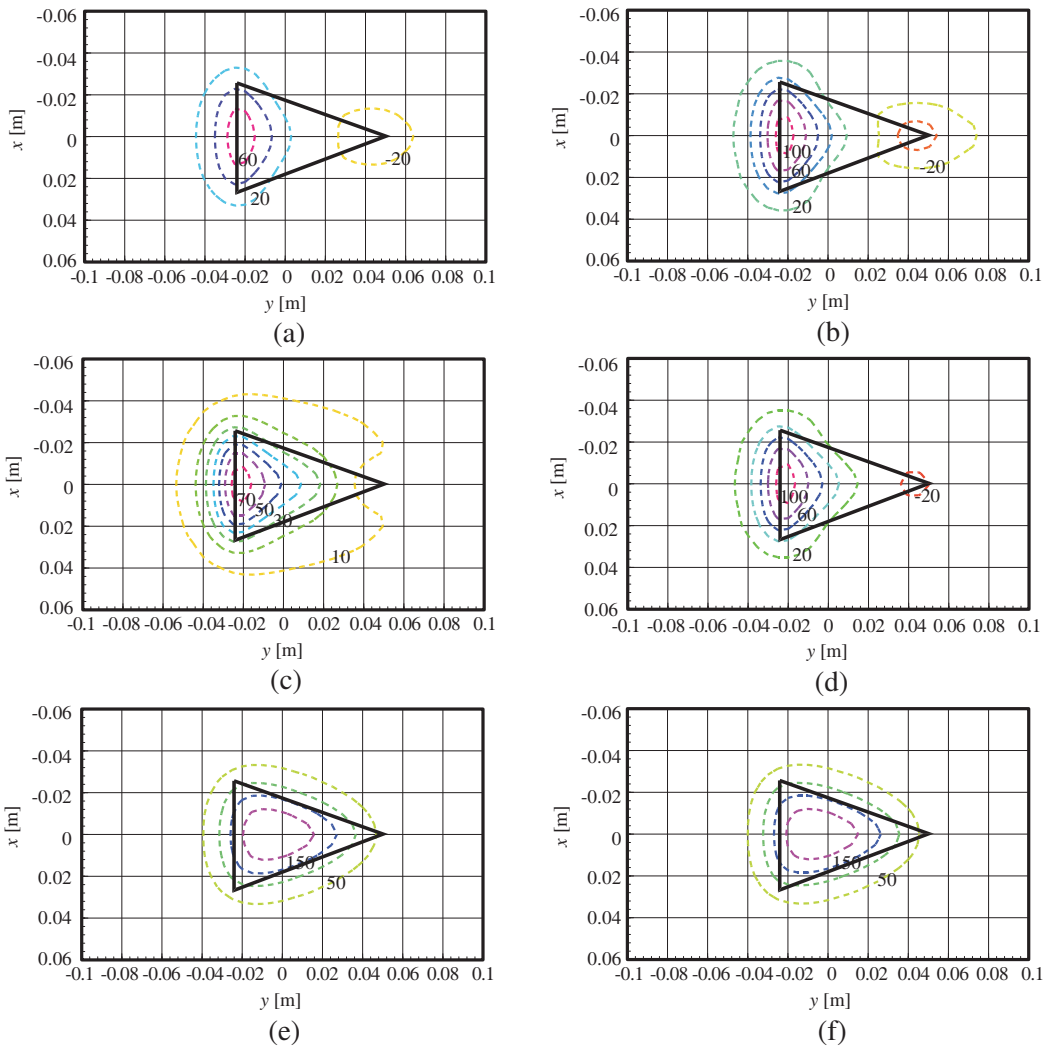

Figure 8. ECDs for a triangular coil when excitation frequency and conductor speed change. (a) DC, $v = 10\,\text{m/s}$, (b) DC, $v = 20\,\text{m/s}$, (c) $f = 100\,\text{Hz}$, $v = 10\,\text{m/s}$, (d) $f = 100\,\text{Hz}$, $v = 20\,\text{m/s}$, (e) $f = 1000\,\text{Hz}$, $v = 10\,\text{m/s}$ and (f) $f = 1000\,\text{Hz}$, $v = 20\,\text{m/s}$.

Figure 8 shows ECD for a triangular coil. At DC and $v = 10\,\text{m/s}$ or $20\,\text{m/s}$, two current vortexes with different polarities were generated in the y-direction. At $f = 100\,\text{Hz}$ and $v = 10\,\text{m/s}$, the current vortex was greatly distorted in the y-direction. At $v = 20\,\text{m/s}$, two current vortexes with opposite polarities were generated in the y-direction. At $f = 1000\,\text{Hz}$, the size of the eddy current increased, but the speed did not affect the ECD. At this frequency, only a single vortex was generated and had a smooth shape with rounded corners of the coil.

Consequently, it is considered that the eddy current generated in the moving conductor slab is composed of current induced by the excitation frequency and conductor speed. When the eddy current generated by the conductor speed is dominant (e.g., at $f = 100\,\text{Hz}$ and $20\,\text{m/s}$), one current vortex is produced in the region of the conductor slab close to the coil. It is generated in the direction that reduces magnetic flux from the coil. The other current vortex is produced in the region of the conductor slab away from the coil, and it is generated in the direction that increases magnetic flux from the coil. Similar results were obtained with the DC excitation current. When the eddy current generated by the excitation frequency is dominant (e.g., at $f = 1000\,\text{Hz}$ and $10\,\text{m/s}$ or $20\,\text{m/s}$), the impact of moving speed is reduced and largely negligible.

4. CONCLUSION

In this study, we derive an exact theoretical solution that visualizes ECD for an arbitrarily shaped coil arranged parallel to a conductor slab, a problem that heretofore remains unsolved. We determine that the eddy current flow in the conductor depends on the excitation frequency and speed of the conductor slab relative to the coil. The visualized ECD in the conductor, which is necessary to advance eddy current testing, induction heating and eddy current sensing, can be obtained from this new analysis.

APPENDIX A.

From Equations (1)–(3), (5) and (6), the magnetic density $\bar{B}$ in the moving conductor slab (this region is defined by $-d < z < 0$ and coincides with the conductor itself) is obtained as follows [13]

$$\nabla^2 \bar{B} - \sigma\mu v_x \frac{\partial \bar{B}}{\partial x} - \sigma\mu v_y \frac{\partial \bar{B}}{\partial y} - j\omega\sigma\mu\bar{B} = \bar{0} \tag{A1}$$

Using Equation (7), Fourier transform of Equation (A1) gives

$$\frac{\partial^2 \bar{b}}{\partial z^2} - \left(\xi^2 + \eta^2 - j\sigma\mu v_x \xi - j\sigma\mu v_y \eta + j\omega\sigma\mu\right)\bar{b} = \bar{0} \tag{A2}$$

Solving the above equation, the x-, y- and z-components of the magnetic flux density $\bar{b}$ in the conductor slab are given by [13]

$$b_x = C_x e^{\gamma z} + D_x e^{-\gamma z} \tag{A3}$$
$$b_y = C_y e^{\gamma z} + D_y e^{-\gamma z} \tag{A4}$$
$$b_z = C_z e^{\gamma z} + D_z e^{-\gamma z} \tag{A5}$$

where

$$\gamma = \sqrt{\xi^2 + \eta^2 - j\sigma\mu\left(v_x\xi + v_y\eta\right) + j\omega\sigma\mu} \tag{A6}$$

The coefficients C_x, C_y, C_z, D_x, D_y and D_z in Equations (A3)–(A5) are obtained as follows [13]

$$C_x = \frac{\mu_r}{1 - e^{2\gamma d}} \left\{ -\left(1 + \lambda_0\right) e^{2\gamma d} + \nu_0 e^{\left(\gamma - \sqrt{\xi^2+\eta^2}\right)d} \right\} C_{ix} \tag{A7}$$

$$C_y = \frac{\mu_r}{1 - e^{2\gamma d}} \left\{ -\left(1 + \lambda_0\right) e^{2\gamma d} + \nu_0 e^{\left(\gamma - \sqrt{\xi^2+\eta^2}\right)d} \right\} C_{iy} \tag{A8}$$

$$C_z = \frac{\mu_r}{1 - e^{2\gamma d}} \left\{ -\left(1 + \lambda_0\right) e^{2\gamma d} + \nu_0 e^{\left(\gamma - \sqrt{\xi^2+\eta^2}\right)d} \right\} \frac{\sqrt{\xi^2+\eta^2}}{\gamma} C_{iz} \tag{A9}$$

$$D_x = \frac{\mu_r}{1 - e^{2\gamma d}} \left\{ 1 + \lambda_0 - \nu_0 e^{\left(\gamma - \sqrt{\xi^2+\eta^2}\right)d} \right\} C_{ix} \tag{A10}$$

$$D_y = \frac{\mu_r}{1 - e^{2\gamma d}} \left\{ 1 + \lambda_0 - \nu_0 e^{\left(\gamma - \sqrt{\xi^2+\eta^2}\right)d} \right\} C_{iy} \tag{A11}$$

$$D_z = -\frac{\mu_r}{1 - e^{2\gamma d}} \left\{ 1 + \lambda_0 - \nu_0 e^{\left(\gamma - \sqrt{\xi^2+\eta^2}\right)d} \right\} \frac{\sqrt{\xi^2+\eta^2}}{\gamma} C_{iz} \tag{A12}$$

where $\mu_r = \mu/\mu_0$. The coefficients C_{ix}, C_{iy} and C_{iz} are determined by the coil geometry. Equations (A7)–(A12) are determined from boundary conditions.

As shown in Figure 1, when an arbitrarily shaped coil, which is positioned at $z = z_0$ and carrying current I, the x-, y- and z-components of magnetic flux density $\bar{b}_i(\xi, \eta, z)$ at $z < z_0$ are described as follows [14]

$$b_{ix} = \frac{\mu_0 I \xi}{2\eta} e^{(z - z_0)\sqrt{\xi^2+\eta^2}} \sum_{i=1}^{n} \int_{x_{i-1}}^{x_i} e^{j\{x\xi + f_i(x)\eta\}} dx = C_{ix} e^{z\sqrt{\xi^2+\eta^2}} \tag{A13}$$

$$b_{iy} = \frac{\mu_0 I}{2} e^{(z-z_0)\sqrt{\xi^2+\eta^2}} \sum_{i=1}^{n} \int_{x_{i-1}}^{x_i} e^{j\{x\xi+f_i(x)\eta\}} dx = C_{iy} e^{z\sqrt{\xi^2+\eta^2}} \tag{A14}$$

$$b_{iz} = j\frac{\mu_0 I\sqrt{\xi^2+\eta^2}}{2\eta} e^{(z-z_0)\sqrt{\xi^2\eta+\eta^2}} \sum_{i=1}^{n} \int_{x_{i-1}}^{x_i} e^{j\{x\xi+f_i(x)\eta\}} dx = C_{iz} e^{z\sqrt{\xi^2+\eta^2}} \tag{A15}$$

Therefore, using shape function $S(\xi, \eta)$ yields

$$C_{ix} = \frac{\mu_0 I\xi}{2\eta} e^{-z_0\sqrt{\xi^2+\eta^2}} S(\xi, \eta) \tag{A16}$$

$$C_{iy} = \frac{\mu_0 I}{2} e^{-z_0\sqrt{\xi^2+\eta^2}} S(\xi, \eta) \tag{A17}$$

$$C_{iz} = j\frac{\mu_0 I\sqrt{\xi^2+\eta^2}}{2\eta} e^{-z_0\sqrt{\xi^2+\eta^2}} S(\xi, \eta) \tag{A18}$$

From Equations (A3)–(A5) and (A7)–(A12), the x-, y- and z-components of magnetic flux density $\bar{b}(\xi, \eta, z)$ at the moving conductor slab are described as follows

$$b_x = \frac{\mu_r}{1-e^{2\gamma d}}\left[\left\{-(1+\lambda_0)e^{2\gamma d}+\nu_0 e^{\left(\gamma-\sqrt{\xi^2+\eta^2}\right)d}\right\}e^{\gamma z}+\left\{1+\lambda_0-\nu_0 e^{\left(\gamma-\sqrt{\xi^2+\eta^2}\right)d}\right\}e^{-\gamma z}\right]C_{ix} \tag{A19}$$

$$b_y = \frac{\mu_r}{1-e^{2\gamma d}}\left[\left\{-(1+\lambda_0)e^{2\gamma d}+\nu_0 e^{\left(\gamma-\sqrt{\xi^2+\eta^2}\right)d}\right\}e^{\gamma z}+\left\{1+\lambda_0-\nu_0 e^{\left(\gamma-\sqrt{\xi^2+\eta^2}\right)d}\right\}e^{-\gamma z}\right]C_{iy} \tag{A20}$$

$$b_z = \frac{\mu_r}{1-e^{2\gamma d}}\left[\left\{-(1+\lambda_0)e^{2\gamma d}+\nu_0 e^{\left(\gamma-\sqrt{\xi^2+\eta^2}\right)d}\right\}e^{\gamma z}-\left\{1+\lambda_0-\nu_0 e^{\left(\gamma-\sqrt{\xi^2+\eta^2}\right)d}\right\}e^{-\gamma z}\right]\frac{\sqrt{\xi^2+\eta^2}}{\gamma}C_{iz} \tag{A21}$$

By using Equations (A16)–(A18) and (8), the inverse Fourier transform of Equations (A19)–(A21) gives Equations (9)–(11).

REFERENCES

1. Mizukami, K., Y. Mizutani, A. Todoroki, and Y. Suzuki, "Detection of delamination in thermoplastic CFRP welded zones using induction heating assisted eddy current testing," *NDT and E Int.*, Vol. 74, 106–111, 2015.
2. Vyroubal, D., "Impedance of the eddy-current displacement probe: The transformer model," *IEEE Trans. Instrum. Meas.*, Vol. 53, No. 2, 384–391, 2004.
3. Chen, X. and Y. Lei, "Electrical conductivity measurement of ferromagnetic metallic materials using pulsed eddy current method," *NDT and E Int.*, Vol. 75, 33–38, 2015.
4. Chen, X. and Y. Lei, "Excitation current waveform for eddy current testing on the thickness of ferromagnetic plates," *NDT and E Int.*, Vol. 66, 28–33, 2014.
5. Musolino, A., R. Rizzo, and E. Tripodi, "A quasi-analytical model for remote field eddy current inspection," *Progress In Electromagnetics Research M*, Vol. 26, 237–249, 2012.
6. Dodd, C. V. and W. E. Deeds, "Analytical solutions to eddy-current probe-coil problems," *J. Appl. Phys.*, Vol. 39, No. 6, 2829–2838, 1968.
7. Panas, S. M. and A. G. Papayiannakis, "Eddy currents in an infinite slab due to an elliptic current excitation," *IEEE Trans. Magn.*, Vol. 27, No. 5, 4328–4337, 1991.
8. Burke, S. K., "Impedance of a horizontal coil above a conducting half-space," *J. Phys. D: Appl. Phys.*, Vol. 19, No. 7, 1159–1173, 1986.
9. Theodoulidis, P. T., "Analytical model for tilted coils in eddy-current nondestructive inspection," *IEEE Trans. Magn.*, Vol. 41, No. 9, 2447–2454, 2005.
10. Theodoulidis, P. T. and E. E. Kriezis, "Impedance evaluation of rectangular coils for eddy current testing of planar media," *NDT and E Int.*, Vol. 35, No. 6, 407–414, 2002.
11. Antonopoulos, C. S. and E. E. Kriezis, "Force on a parallel circular loop moving above a conducting slab and the eddy-current distribution," *IEE Proceedings A*, Vol. 133, No. 9, 601–605, 1986.

12. Panas, S. M. and E. E. Kriezis, "Eddy current distribution due to a rectangular current frame moving above a conducting slab," *Archiv für Elektrotechnik*, Vol. 69, No. 3, 185–191, 1986.
13. Itaya, T., K. Ishida, A. Tanaka, N. Takehira, and T. Miki, "Eddy current distribution for a rectangular coil arranged parallel to a moving conductor slab," *IET Sci. Meas. Technol.*, Vol. 6, No. 2, 43–51, 2012.
14. Ishida, T., T. Itaya, A. Tanaka, and N. Takehira, "Magnetic field analysis of an arbitrary shaped coil using shape functions," *IEEE Trans. Magn.*, Vol. 45, No. 1, 104–112, 2009.